Supporting information

An Edge-decorated Submicron Reduced Graphite Oxide Nanoflakes and Its Composites with Carbon Nanotubes for Transparent Conducting Films

By Rui Su[a], Wei Fu Sun[b], Cheng Tian[a], Wei Ming Huang[a], Shao Fen Lin [a], Dan Qing Chen[a], Guo Hua Chen*[a]

[a] Department of Polymer Science & Engineering, Huaqiao University, Xiamen, 361021, China. E-mail: hdcgh@hqu.edu.cn;

Fax: +86-592-6166296; Tel: +86-592-6162280

[b] School of Materials Science & Engineering, University of New South Wales, Sydney, NSW 2052, Australia.

1. Experimental details

Graphite oxide (GO) was synthesized by Hummers method [1] from graphite powder (500 mesh, Sinopharm) and dried at 45 °C for 48 hours. Reduced graphite oxide (RGO) was prepared by placing GO into a microwave oven (Midea, China) for 20 seconds at a power of 700 W. A series of identical RGO dispersions were prepared by adding RGO powder to NMP (content > 98%, Xilong) at a concentration of 2.5 mg/mL. RGO dispersions were then put into jars of a planetary ball-mill machine ball milling for various periods from 48 to 120 hours. Afterwards, samples were centrifuged at 6000 rpm for 10 minutes and the clarified liquid was got carefully. Then the clarified liquid was heated to 200 °C and washed by water repeatedly to remove NMP. The as-obtained submicro-sized reduced graphite oxide (μRGO) nanoflakes were re-dispersed in water at a series of concentration ranging from 0.25 to 0.5 mg/mL(**scheme S1**). Multiwalled carbon nanotubes (MWNTs) (content > 95%, Chengdu Organic Chemicals) were added into the μRGO dispersion without any post-

treatment and the weight ratio of μRGO flakes and MWNTs is fixed at 1:1. After sonication at a power of 100W for 1 hour, stable hybrid dispersion was formed.

The used quartz substrates (1.5×1.5 cm^2) were successively cleaned by 20% HCl, 30% NaOH and alcohol. Then the hybrid dispersion was deposited onto those quartz substrates. The quartz substrates were completely covered with μRGO/MWNTs hybrid dispersion, followed by being subjected to spin-coating at 100 rpm for 2 seconds. Then the substrate was dried at 90 °C in a convection oven for 30 minutes to obtain the transparent conducting film.

Instruments: UV-vis absorption spectra and transmittance were measured using a UV-1600 Spectrophotometer (Beijing Rayleigh Analytical Instruments). Transmission electron microscopy (TEM) images were taken by a JEM-2010 JEOL transmission electron microscope. High-resolution TEM (HR-TEM) images were taken by an H-7650 (HITACHI). Atomic force microscopy (AFM) images were collected on a Nanoscope Multimode IIIa scanning probe microscopy system (Veeco Instruments Ltd) in tapping mode. X-ray photoelectron spectroscopy (XPS) was recorded on a VG Escalab MK II spectrometer (Scientific Ltd). Thermogravimetric analysis were conducted on TA Instruments DTG-60H (Shimadzu)at a heating rate of 10 °C/min. X-ray diffraction (XRD) patterns were recorded with a D8-Advance instrument (Bruker AXS) using Cu-Ka radiation generated at a voltage of 40 kV and a current of 40 mA from 5° to 40° of 2θ range with a scanning rate of 2 °/min. Raman spectra were taken with a He− Ne laser (532 nm) as the excitation source by using Labram spectrometer (Super LabRam II system). Sheet resistivity of film was measured using four point probe instrument.
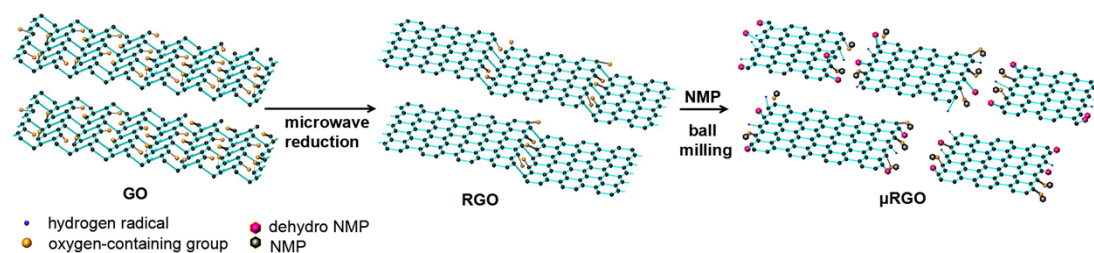
Scheme S1 Preparation of μRGO dispersions

2. Optimization of manufacturing processes

Briefly, RGO together with N-methyl-pyrrolidone (NMP) were ball-milled for 96 hours, followed by being centrifuged at 6000 rpm. Then we explain how to determine the process parameters.

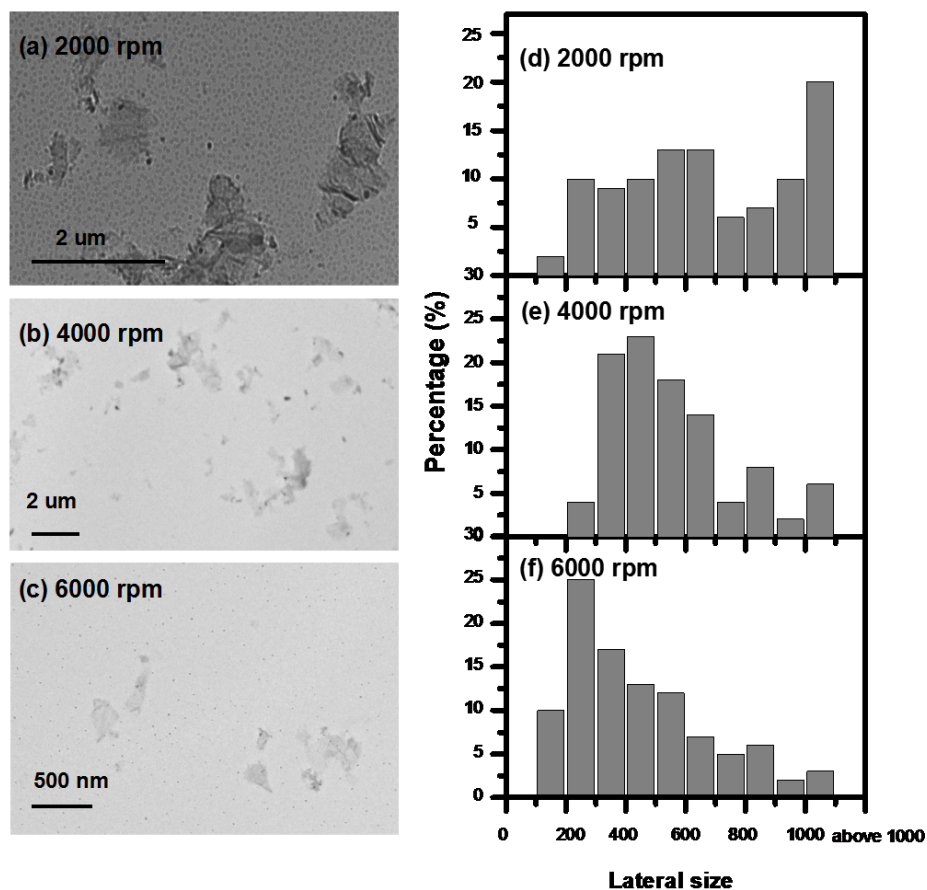### 2.1 Lateral size of flakes as a function of centrifugal rate

Fig. S1 The TEM images (left) and the corresponding lateral size (right) of flakes as a function of centrifugal rate at (a) and (d) 2000 rpm; (b) and (e) 4000 rpm; (c) and (f) 6000 rpm.

Centrifugation here is used to remove large micron-sized and multilayer flakes. Fig. S1 gives the relationship between μRGO flake sizes and centrifugation rates. We find that the fractions of flakes ≤ 500 nm are 31%, 48% and 65% at the centrifugation rate 2000 rpm, 4000 rpm and 6000 rpm, respectively. It can be noted that centrifugation process preferentially removes the larger flakes.

2.2 Concentration after centrifugation as a function of ball milling time
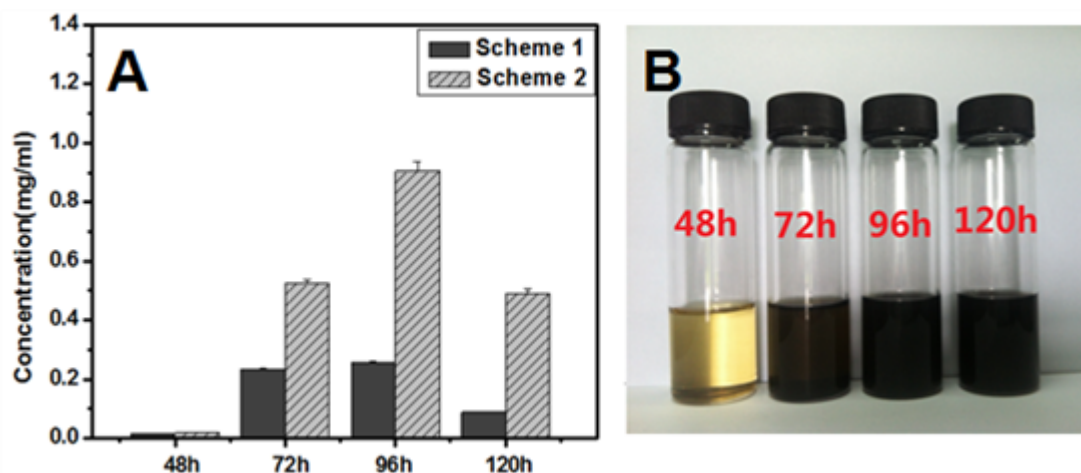

Fig. S2 A) The concentration after centrifugation as a function of the ball milling time under both schemes. **B)** Photos of μRGO dispersions as a function of ball milling time under scheme 2.

In most cases there's a practical size limit in ball milling system. So extending the time excessively is high-cost. Our method for preparing this kind of RGO dispersion requires high-speed centrifugation (6000 rpm for 10 min) after the use of ball milling. When considering optimization of dispersion conditions, we discuss two factors: the ratio of balls of different sizes and ball milling time. The optimum ball milling parameters will increase concentration of centrifugal liquid. The concentration is measured through the Lambert-Beer law, $A=\alpha cl$ [2-3]. We found that the absorption coefficient is different with changing of processing parameters (**Fig. S3**). Compared with absorption coefficient measured for graphene in NMP, $\alpha=2460$ mL mg^{-1}m^{-1}, μRGO increases the value of α by almost 3 orders of magnitude mainly due to the presence of oxygen functional groups.

The ball milling process is applied to generate μRGO flakes with abundant surface defects, esp. the edge defects in present case. But no regular relationship between ball milling time and the lateral size of the flakes is found. However, we do find a relationship between concentration after centrifugation and ball milling time. By increasing the ball-milling time, the concentration first increases gradually to a

peak and then decreases.

Fig. S2A shows concentration after centrifugation as a function of ball milling time. With ball-milling time the concentration has an obvious rise and fall. From 48h to 96h, concentration increase from 0.018 to 0.905 mg/mL. It indicates that flaks are grinded sufficiently gradually in this process. The value 0.905 mg/mL of high concentration is got after such a high-speed centrifugation (6000 rpm for 10 mins) indicating that flakes in NMP are quite stable. But at 120 h, concentration decreases to 0.490 mg/mL because of flakes agglomeration. Photos of μRGO dispersions as a function of ball milling time also showed in Fig. S2B. Our samples prepared ten months ago show no signs of precipitation.
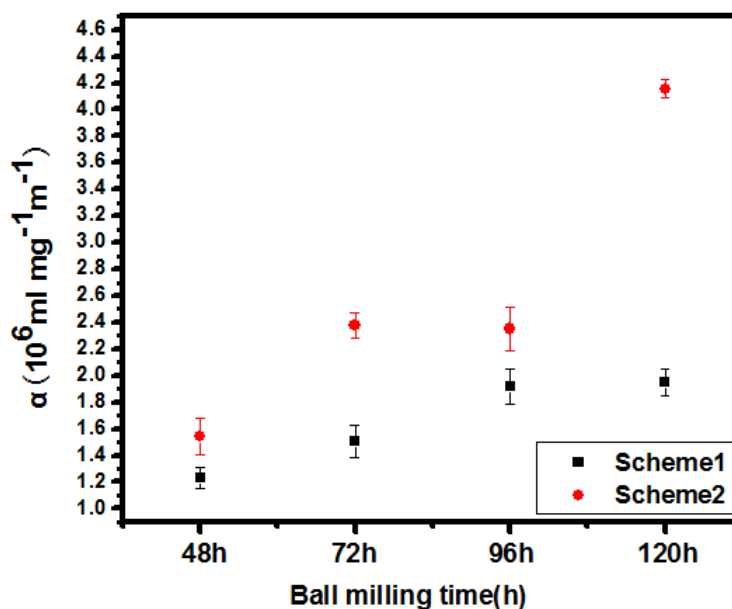

Fig. S3 The absorption coefficient as a function of ball milling time under both schemes.

We create two schemes adjusting the ratio of balls of different sizes. We select more tiny balls which sizes are between 0.4 mm and 0.6 mm under scheme 1 than scheme 2. The calculated concentrations after centrifugation under both schemes are shown in Fig. S2A. We find that the concentration under scheme 2 is much higher than that in scheme 1 entirety after the same ball-milling time. This can be interpreted as too many tiny balls can not exfoliate the flakes well in high-speed rotating. Besides, under scheme 1 there is limited space around tiny balls. The dispersion is easy to

achieve a local high concentration and viscosity. So we prefer scheme 2 for further study.

3. High concentration of the µRGO dispersion

Compared with other's work [4], it is not surprising that µRGO dispersion can reach a high concentration of 15 mg/mL in NMP without CNTs due to very small area of flakes and residual NMP around the flakes. Pure µRGO can also maintain a high concentration (at least 10 mg/mL) in water. As shown in Fig. S2A, 0.905 mg/mL is got after a high-speed centrifugation (6000 rpm for 10 mins), indicating that flakes in NMP are quite stable. Such high stability favors multiwalled carbon nanotubes (MWNTs) to disperse in polar solvents whereas pure MWNTs will sediment in water.

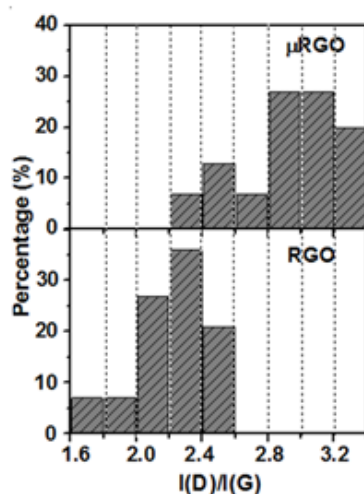## 4. Distribution of I(D)/I(G) of µRGO and RGO

Fig. S4 Distribution of I(D)/I(G) of µRGO and RGO. The I(D)/I(G) of RGO and µRGO are in a range of 1.6−2.6 and 2.2−3.4 respectively. Due to increase of edges, µRGO shows high defect content.
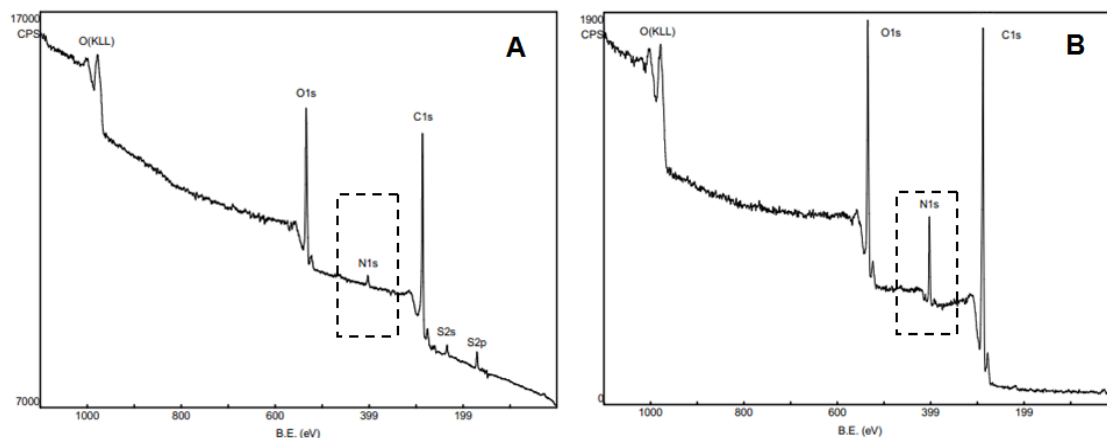
5. XPS spectra of the RGO and µRGO

Fig. S5 XPS survey spectra of the RGO (A) and μRGO (B). There is only a trace amount of N (approximately 300 eV) in RGO spectra while the N 1 s peak intensity relative to the C 1 s peak in μRGO spectra increases significantly indicating NMP molecule has been introduced to the μRGO flakes.

6. The ratio of μRGO and MWNTs for films

When we keep the μRGO and MWNTs at ratios of 2:1, 1:1 and 1:2, the sheet resistances for the films are 1300, 152 and 105 Ω/square with the same transmittance of 84%, respectively. That is to say, the lower content of MWNTs will cause an eminent increase in sheet resistance. While for higher content of MWNTs, sheet resistance has not significantly decreased and in the μRGO-MWNTs composite dispersion precipitate of excess MWNTs appears. So it is appropriate to keep μRGO and MWNTs at a ratio of 1:1.

7. The FTIR spectrum of GO, RGO and μRGO

The spectrum of GO show the presence of O-H stretching at 3430 cm^{-1}, C=O stretching at 1723 cm^{-1}, C-OH stretching at 1230cm^{-1}, C-O stretching at 1050cm^{-1} and C=C vibrations at 1625cm^{-1}.[5] It indicates that there are -COOH, -OH and -C-O-C- groups on GO flakes.

After microwave-reduction, most of the characteristic features of GO disappeared and only O-H stretching at 3452 cm^{-1} and C=C vibrations at 1633 cm^{-1} still exist in the

spectrum of RGO. This can be explained by that -COOH groups had been removed and some -OH groups at the edge are hard to be reduced.

After ball-milling, however, a set of new peaks arose, which could be attributed to (N-CH$_3$) 1114 cm^{-1}, (C-N)1291 cm^{-1} and (C=O) 1715 cm^{-1} stretches of grafted NMP [6,7]. The peak at 1633 cm^{-1} and at 3438 cm^{-1} represent C=C vibrations and O-H stretching, respectively.
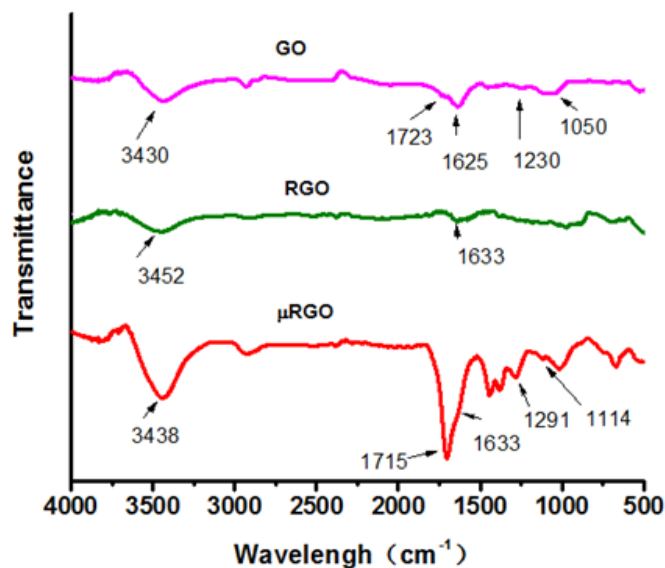

Figure S6 FTIR of GO, RGO and μRGO.

8. TEM images of GO

Figure S7 TEM images of GO. The sizes of GO flakes are above 1μm.
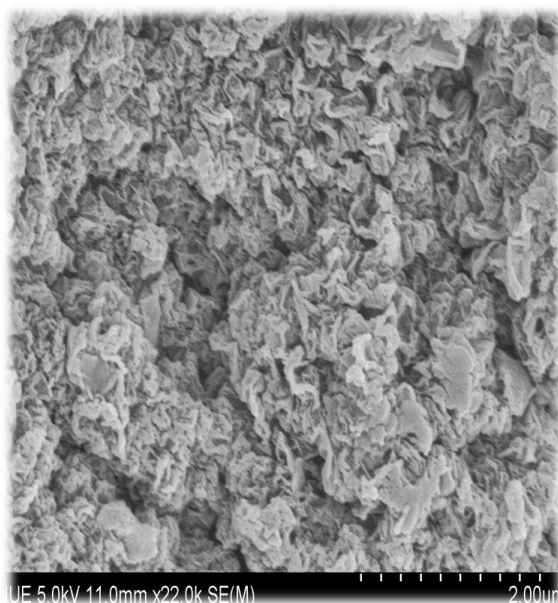
9. The SEM images of nano RGO flakes

Figure S8 The SEM images of nano RGO flakes.

10. Density function theory (DFT) calculation

All the details of DFT calculations can be seen in the supporting information of Ref.8.

References:

[1] W. S. Hummers and R. E. Offeman, *J. Am. Chem. Soc.*1958, **80**, 1339.

[2] M. Lotya, P. J. King, U. Khan, S. De and J. N. Coleman, *ACS Nano,* 2010, **4**, 3155.

[3] U. Khan, A. O'Neill, M. Lotya, S. De and J.N. Coleman, *Small* 2010, **6**, 864.

[4] F. J. Tölle, M. Fabritius and R. Mülhaupt, *Adv. Funct. Mater.,* 2012, **22**, 1136.

[5] S. Stankovich, R. D. Piner, S. B. T. Nguyen and R. S. Ruoff, *Carbon*, 2006, **44**, 3342.

[6] J. Y. Niu, M. L. Wei, J. P. Wang and D. B. Dang, *Eur. J. Inorg. Chem*, 2004, **1**, 160.

[7] M. Tabbal, P. Merel,S. Moisa, M. Chaker, E. Gat, A. Ricard, M. Moisan and S. Gujrathi, *Surf. Coat. Tech*, 1998, **98**, 1092.

[8] R. Su, S. F. Lin, D. Q. Chen and G. H. Chen, *J. Phys. Chem. C*, 2014, **118**, 12520.